Rise Time Reduction of Thermal Actuators Operated in Air and Water through Optimized Pre-Shaped Open-Loop Driving

T. Larsen,[1)] J. C. Doll,[1)] F. Loizeau,[1)] N. Hosseini,[2)] A. W. Peng,[3)] G. Fantner,[2)] A. J. Ricci,[3)] and B. L. Pruitt[1)]

[1]*Department of Mechanical Engineering, Stanford University, Stanford, California, 94305, USA.*

[2]*Laboratory for Bio- and Nano-Instrumentation, École Polytechnique Fédérale de Lausanne, Batiment BM 3109 Station 17, 1015 Lausanne, Switzerland.*

[3]*Department of Otolaryngology, Head and Neck Surgery, Stanford University, Stanford, California, 94305, USA.*

Electrothermal actuators have many advantages compared to other actuators used in Micro-Electro-Mechanical Systems (MEMS). They are simple to design, easy to fabricate and provide large displacements at low voltages. Low voltages enable less stringent passivation requirements for operation in liquid. Despite these advantages, thermal actuation is typically limited to a few kHz bandwidth when using step inputs due to its intrinsic thermal time constant. However, the use of pre-shaped input signals offers a route for reducing the rise time of these actuators by orders of magnitude. We started with an electrothermally actuated cantilever having an initial 10-90% rise time of 85 μs in air and 234 μs in water for a standard open-loop step input. We experimentally characterized the linearity and frequency response of the cantilever when operated in air and water, allowing us to obtain transfer functions for the two cases. We used these transfer functions, along with functions describing desired reduced rise-time system responses, to numerically simulate the required input signals. Using these pre-shaped input signals, we improved the open-loop 10-90% rise time from 85 μs to 3 μs in air and from 234 μs to 5 μs in water, an improvement by a factor of 28 and 47, respectively. Using this simple control strategy for MEMS electrothermal actuators makes them an attractive alternative to other high speed micromechanical actuators such as piezoelectric stacks or electrostatic comb structures which are more complex to design, fabricate, or operate.

1. Introduction

Electrothermal actuators have been extensively used in low-speed MEMS applications due to their ease in design, implementation, operation, and large displacements at low voltages [1]. These features have been of particular interest for actuation in liquid or biological environments [2, 3]. Electrothermal actuator applications have included: micro-grippers [4], micro-scale tensile testing [5], switches [6, 7], scanning probes [8-13], resonators [14], micro-mirrors [15], etc. Thermal actuation has been achieved with single material configurations, e.g. hot/cold arms or buckling structures, and with bimorph configurations [16]. In both cases, the bandwidth has been limited by the time it takes to heat up or cool down the structures. Minimizing this thermal time constant has relied on reducing heat capacity and/or increasing the thermal conductance of the actuator. Despite this, state-of-the-art electrothermally actuated scanning probes have been reported with bandwidths only up to 0.3-11 kHz [9-13], significantly slower than other actuation technologies. For comparison, we have previously demonstrated piezoelectric actuated cantilevers with actuation bandwidths limited by their mechanical resonance of ~300 kHz [17].

The dynamics of a cantilever actuator scales with physical size, i.e., fast actuation requires small cantilevers. Piezoelectric actuators require large drive voltages which necessitate thick dielectric passivation against breakdown in liquid; thus their design and operation are limited by tradeoffs between the thickness, stiffness, and breakdown voltage of conventional passivation films such as Parylene or oxides. Thus, we revisited the dynamics of thermal actuators and investigated the use of pre-shaped input signals to systematically reduce the rise time of a simple step actuation of a electrothermally actuated cantilever operated in air and water. Thermal actuator dynamics are described by a transient phase governed by the thermal time constant as the structure heats up, followed by a steady-state phase where the energy inflow and heat loss balance each other. For linear actuators an overshoot in the transient phase can be utilized to achieve an effectively shorter rise time. In closed-loop operation, a well-tuned feedback controller can deliver the input signals required to reduce rise times [18]. However, the physical size of MEMS and constraints from application environments present unique challenges for integrating a feedback sensor. Short time constants in control loops also present challenges for typical digital controllers and require high sampling rates [19]. For these reasons, we present an open-loop approach for tuning the actuation of MEMS thermally actuated cantilevers. By leveraging a model of the system dynamics, pre-shaped input signals can decrease the rise time by more than an order of magnitude [7, 15, 18, 20, 21].

We first present a detailed system identification of an electrothermally actuated cantilever operated in air and water. By combining our model transfer functions with functions describing the desired responses of the actuator, we numerically

simulate the requisite pre-shaped input signal. Finally, we apply the pre-shaped input signals, measure the cantilever tip responses, and compare them to our predictions.

2. Experimental Details

The electrothermally actuated cantilever (Figure 1) was fabricated using a silicon-on-insulator process previously reported in [13]. The cantilever structure consists of two-parts, 1) a piezoresistive sensing cantilever (300 nm thick, 28 µm long and 2 µm wide) at the tip, not used in this work but which affects system dynamics, and 2) a wider electrothermal actuating cantilever (1.45 µm thick, 50 µm long, and 20 µm wide). The integrated heater is a loop of doped silicon separated by an air-gap and has a resistance of ~4.5 kΩ. No passivation layer is needed for operation in air. For operation in water we passivated the cantilever with a 310 nm thick layer of Parylene N; this film changes the stiffness from k = 72 to 407 mN/m and natural frequency from $\omega_0/2\pi$ = 299 to 403 kHz.

Though the demonstrations of rise time reduction in air and water were done sequentially, we describe the steps for the air and water systems in parallel as the main steps are identical. We first measured the frequency response of cantilever velocity using a Polytec laser Doppler vibrometer (LDV) (OFV-534/OFV-2500-1) and an HP 89441A vector signal analyzer. The data were then integrated to obtain displacement data from velocity data. Cantilever tip displacement, in time space, was determined by acquiring the LDV velocity signal using an HP Infinium oscilloscope and integrating the signal over time. The input drive signals were generated and applied using a Tektronix AFG3102 arbitrary function generator.

3. Results and Discussion

We investigated system linearity by measuring the static tip displacement for different levels of power dissipation in the heater (Figure 2). In both air and water, the cantilever showed a linear behavior allowing us to described the two cases as linear and time-invariant systems. The tip displacement per dissipated power was 251 nm/mW in air. This was reduced to 114 nm/mW when operating the cantilever in water because the Parylene N coating stiffened the cantilever and operation in water increased the heat loss.

We measured frequency responses and fitted transfer functions for operation in air and water (Figure 2). For these measurements, we drove the thermal actuator with a periodic chirp signal, amplitude 0.2 V and offset 2 V. The DC offset was introduced to have a linear component of the actuation. We fitted transfer functions to the magnitude and phase as a function of the power dissipation at the AC input frequency. The overall approach follows the one described in details in reference [10]. For the cantilever operated in air, three distinct regimes were identified: (i) at low frequencies the magnitude response is flat and the system is able to follow the applied input signal without attenuation, (ii) above ~4 kHz, the amplitude is

attenuated due to the finite thermal time constant of the actuator, and (iii) at high frequencies, underdamped mechanical resonances emerge at 299 kHz and 610 kHz, respectively. The behavior for electrothemally actuated cantilevers has been modeled and described in detail previously [13, 22]. Finite element simulations confirm that the two resonances correspond to the first two flexural bending modes of the cantilever structure. The measured frequency response is fitted using a model composed of 6 parts: (i) a gain (243 nm/mW) describing the DC tip displacement as a function of power dissipated in the actuator, (ii) a first-order response describing the thermal actuation, (iii & iv) two second-order responses describing the two mechanical resonances,(v) a first-order response, one pole and one zero, to better describe the frequency response above 20 kHz and (vi) a first order Padé approximation, one pole and one zero, [23] to fit a time delay observed as a linear slope of the phase response. Thus, the final fitted transfer function included 7 poles and 2 zero described by a 7^{th}-order polynomial, see Table 1 for a complete description of the fitted polynomial. The 10-90% rise time of the system in air was 85 µs.

We followed the same procedure to fit the frequency response of the cantilever actuated in water. The attenuated thermal actuation in water had mechanical resonances at 175 kHz and 296 kHz, and a more complex thermal actuation response fitted with a second-order response with a zero (Figure 2). The fitted transfer function also included a gain (114 nm/mW in water) and again, the addition of a first-order response and a first-order Padé approximation. The fitted transfer function for actuation in water included 8 poles and 3 zeros described by an 8^{th}-order polynomial, again see Table 1 for a complete description of the fitted polynomial). The 10-90% rise time of the system in water was 234 µs.

Using these models and assuming linear system responses, we calculated the input signal, $x(t)$, needed to reduce the rise time of the response to a desired target. $x(t)$ is calculated by taking the inverse Laplace transform of $X(s)$, which is given by the desired response, $Y(s)$, divided by the transfer function of the system, $H(s)$, where t = time and s = complex frequency. We can describe our desired response by first multiplying the system gain with a first-order response described by our target time constant, and then multiplying with a step function. The construction of this function is simple, yet taking the inverse Laplace transform of $Y(s)/H(s)$ is tedious for complex functions. Thus, we iteratively applied the Matlab function *lsim* to numerically simulate the time response of $Y(s)/H(s)$. *lsim* simulates the time response of continuous or discrete linear systems to arbitrary inputs [24]. Shifting to this approach is not without cost as the *lsim* function can only handle simulations where the number of poles is equal to or greater than the number of zeros. Neglecting the time delay in our systems, our desired responses required 5^{th}-order polynomials, for both cases. To construct these higher-order polynomials, we multiply the gain of the system of interest by 5 first-order polynomials. We achieve two advantages by constructing polynomials in this way: (i) we define a critically damped desired response, yielding a response without ringing [25], and (ii) we control the response time by letting one pole dominate the overall response. This is done by placing the remaining poles far to the left in

the s-plane. By sweeping the position of the dominant pole, we sweep a range of desired rise time. A pole-zero map representation of the dominating pole manipulation, for the desired responses in air, can be seen in Figure 3. The lower limit of the rise time is defined by experimental realities such as: (i) break down of the heater at high power dissipation (>20 mW), and (ii) net positive power dissipation, i.e. negative solutions to $x(t)$ emerge mathematically to suppress resonances but are not physically possible in our system. Simulations find these lower limits at 2.7 µs (air) and 2.9 µs (water), limited by the power dissipation constraint.

The experimentally applied input signals and measured cantilever tip displacement are shown in Figure 4 (air) and Figure 5 (water). In air, the cantilever has an underdamped response with high frequency ringing for a step input. In water, the cantilever has a damped response and no ringing for a step input. In both cases, as we swept through our range of pre-shaped inputs $x(t)$ with increasing power ″overshoot″, the 10-90% rise time was gradually reduced to 3 µs (air) and 5 µs (water). The maximum overshoot in displacement increased acceptably to ~3% in air and ~5% in water. The insets in Figure 4 and Figure 5 reveal good agreement between the simulated and measured tip displacement for the shortest rise times.

So far, only reduction of the rise time has been considered. However, some applications require that time for the actuator to return to its initial position is short, too. As the power dissipated in the actuator can′t reach negative values the actuator has to be operated with an offset to allow reduction of the return time. Doing so, it is possible to reduce the return time in the same manner as we have done for the rise time.

Pre-shaped input signals for MEMS actuators have previously been constructed by using a series of well-defined squared pulses of different amplitude [7, 18, 21, 26]. The drawback of this approach is that mechanical ringing of the system is not suppressed by the input signal [18]. However, dividing each step into smaller steps can reduce the mechanical ringing [26]. In our approach, mechanical ringing is directly suppressed by defining a desired output signal that is critically damped. An alternative to the dominating-pole-manipulation approach, used here, is to define an optimization problem in which all the poles are allowed to move [27]. By not constraining 4 of the poles, the lower limit for the rise time could potentially be reduced. Compared to prior work demonstrating a 5 µs rise time of microcantilevers with integrated piezoelectric actuation [17], we demonstrate a system modeling approach for pre-shaped inputs that achieve similar rise times for electrothermally actuated microcantilevers. These electrothermal actuators are easy to fabricate and can generate larger tip deflections using lower input voltages compared to e.g. piezoelectric actuators [17].

4. Conclusions

In conclusion, we have demonstrated a simple approach for decreasing the 10-90% rise time of electrothermally actuated microcantilevers by a factor of 28 in air and 47 in water. We performed detailed system characterization in air and water to verify the linearity of the systems and determine system transfer functions. By constructing desired responses and manipulating pole positions, we numerically simulated pre-shaped input signals to achieve output responses over a target range of reduced rise times. Due to the system's natural resonant modes, the lower limit for practical rise times were estimated to 2.7 μs and 2.9 μs in air and water, respectively. The approach presented here broadens the range of applications for electrothermal actuators but can also be applied to shape the open-loop response for any type of actuator.

Acknowledgements

This work was funded in part by NIH R01 EB 006745, a Stanford Bio-X seed grant (TL), the Swiss National Science Foundation grant P2ELP2_151909 (FL), NIH K99/R00 DC 013299 (AWP) and NIH R01 DC 003896 (AJR), the Swiss National Science Foundation through grant 205320_152675 (NH & GF), the European Union FP7/2007-2013/ERC under Grant Agreement No. 307338-NaMic, and Eurostars E!8213 (NH & GF). The authors would also like to thank A. Nekimken and J. A. Franco for helpful discussions.

References

1. Bell, D.J., et al., *MEMS actuators and sensors: observations on their performance and selection for purpose.* Journal of Micromechanics and Microengineering, 2005. **15**(7): p. S153.
2. Anand, S., et al., *Electrothermal Microactuators With Peg Drive Improve Performance for Brain Implant Applications.* Microelectromechanical Systems, Journal of, 2012. **21**(5): p. 1172-1186.
3. Zhang, W., et al., *A polymer V-shaped electrothermal actuator array for biological applications.* Journal of Micromechanics and Microengineering, 2008. **18**(7): p. 075020.
4. Comtois, J.H. and V.M. Bright. *Surface micromachined polysilicon thermal actuator arrays and applications*. in *Proc. Solid-State Sensor and Actuator Workshop*. 1996.
5. Kapels, H., R. Aigner, and J. Binder, *Fracture strength and fatigue of polysilicon determined by a novel thermal actuator [MEMS]*. Electron Devices, IEEE Transactions on, 2000. **47**(7): p. 1522-1528.
6. Kruglick, E.J. and K.S. Pister, *Lateral MEMS microcontact considerations.* Microelectromechanical Systems, Journal of, 1999. **8**(3): p. 264-271.
7. Czaplewski, D.A., et al., *A soft-landing waveform for actuation of a single-pole single-throw ohmic RF MEMS switch.* Microelectromechanical Systems, Journal of, 2006. **15**(6): p. 1586-1594.
8. Pedrak, R., et al., *Micromachined atomic force microscopy sensor with integrated piezoresistive sensor and thermal bimorph actuator for high-speed tapping-mode atomic force microscopy phase-imaging in higher eigenmodes.* Journal of Vacuum Science & Technology B, 2003. **21**(6): p. 3102-3107.

9. Hafizovic, S., K.-U. Kirstein, and A. Hierlemann, *Integrated cantilevers and atomic force microscopes*, in *Applied Scanning Probe Methods V*. 2007, Springer. p. 1-22.
10. Fantner, G.E., et al., *DMCMN: in depth characterization and control of AFM cantilevers with integrated sensing and actuation.* Journal of dynamic systems, measurement, and control, 2009. **131**(6): p. 061104.
11. Lee, B., C.B. Prater, and W.P. King, *Lorentz force actuation of a heated atomic force microscope cantilever.* Nanotechnology, 2012. **23**(5): p. 055709.
12. Wu, C.-P., et al., *CMOS integrated cantilevers with sub-μm tips for surface temperature measurement.* Journal of Micromechanics and Microengineering, 2007. **17**(12): p. 2432.
13. Doll, J.C. and B.L. Pruitt, *High-bandwidth piezoresistive force probes with integrated thermal actuation.* Journal of Micromechanics and Microengineering, 2012. **22**(9): p. 095012.
14. Lavrik, N.V. and P.G. Datskos, *Femtogram mass detection using photothermally actuated nanomechanical resonators.* Applied Physics Letters, 2003. **82**(16): p. 2697-2699.
15. Pal, S. and H. Xie, *Pre-shaped open loop drive of electrothermal micromirror by continuous and pulse width modulated waveforms.* Quantum Electronics, IEEE Journal of, 2010. **46**(9): p. 1254-1260.
16. Mahameed, R. and D. Elata, *Two-dimensional analysis of temperature-gradient actuation of cantilever beam resonators.* Journal of Micromechanics and Microengineering, 2005. **15**(8): p. 1414.
17. Doll, J.C., et al., *Faster than the speed of hearing: nanomechanical force probes enable the electromechanical observation of cochlear hair cells.* Nano letters, 2012. **12**(12): p. 6107-6111.
18. Borovic, B., et al., *Open-loop versus closed-loop control of MEMS devices: choices and issues.* Journal of Micromechanics and Microengineering, 2005. **15**(10): p. 1917.
19. Chen, K.-S. and K.-S. Ou, *Command-shaping techniques for electrostatic MEMS actuation: analysis and simulation.* Microelectromechanical Systems, Journal of, 2007. **16**(3): p. 537-549.
20. Popa, D.O., et al. *Dynamic modeling and input shaping of thermal bimorph MEMS actuators*. in *Robotics and Automation, 2003. Proceedings. ICRA'03. IEEE International Conference on*. 2003. IEEE.
21. Do, C., et al., *Energy-based approach to adaptive pulse shaping for control of RF-MEMS DC-contact switches.* Microelectromechanical Systems, Journal of, 2012. **21**(6): p. 1382-1391.
22. Lammerink, T.S.J., M. Elwenspoek, and J.H.J. Fluitman, *Frequency-Dependence of Thermal Excitation of Micromechanical Resonators.* Sensors and Actuators a-Physical, 1991. **27**(1-3): p. 685-689.
23. Franklin, G.F., J.D. Powell, and A. Emami-Naeini, *Feedback Control of Dynamic Systems*. 2011: Pearson Education.
24. MATLAB R2013a, T.M., Inc., Natick, Massachusetts, United States.
25. Nise, N.S., *Control Systems Engineering, 7th Edition*. 2015: Wiley.
26. Eun, Y., B. Jeong, and J. Kim, *Switching time reduction for electrostatic torsional micromirrors using input shaping.* Japanese Journal of Applied Physics, 2010. **49**(5R): p. 054102.
27. Popa, D.O., et al., *Dynamic modeling and input shaping for MEMS.* Nsti Nanotech 2004, Vol 2, Technical Proceedings, 2004: p. 315-318.

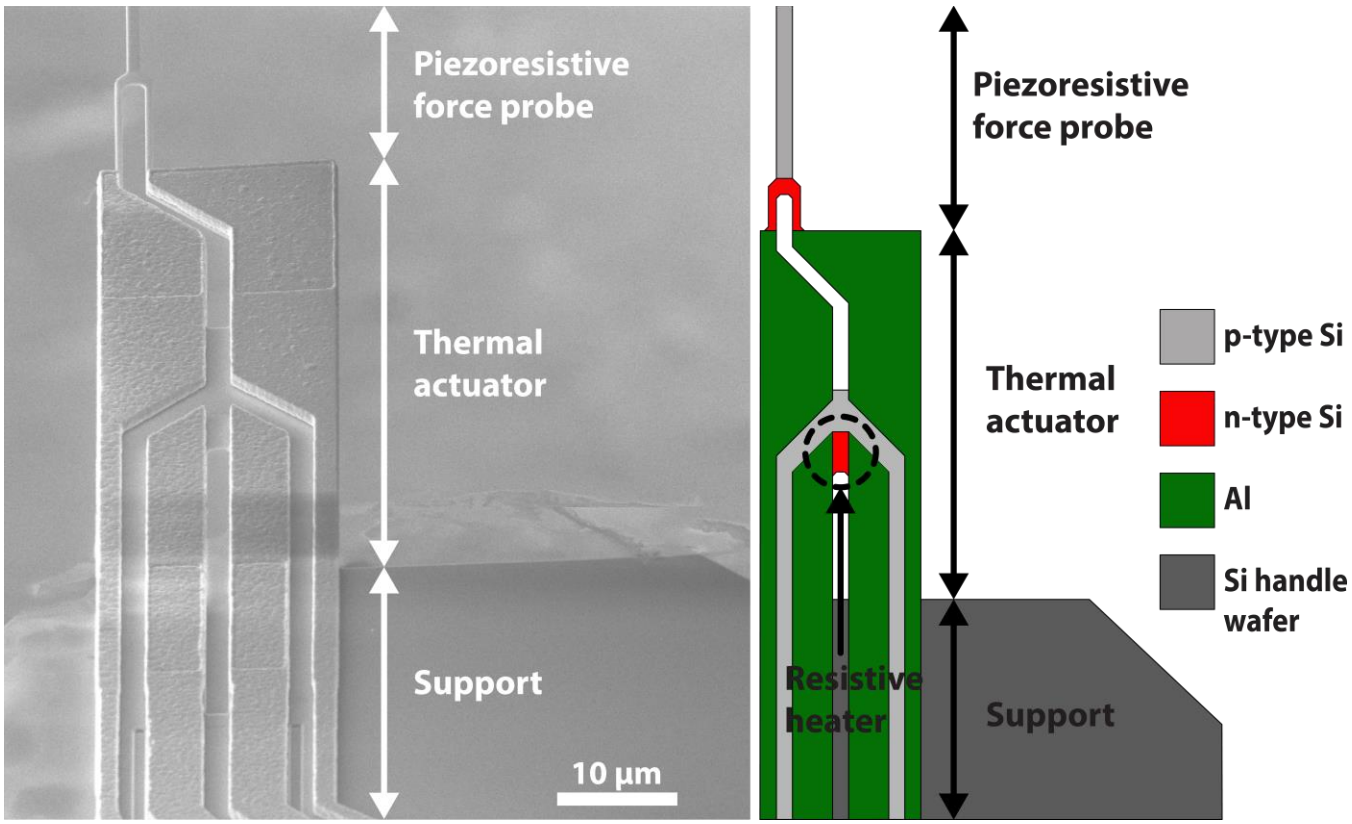

Figure 1: Scanning electron microscope picture and schematic representation of the cantilever, which consists of a narrow force probe with piezoelectric sensing at the end of a wider electrothermal actuator. The piezoresistive force probe is 28 µm long, 2 µm width and 300 nm thick and it is made from p- and n-type silicon. The actuator is 50 µm long, 20 µm wide and 1.45 µm thick and is a layered structure of Si (300 nm)/SiO_2 (100 nm)/Ti (50 nm)/Al (1,000 nm). A ~4.5 kΩ resistive loop formed around a 2 µm wide air gab in the center of the actuator serves as integrated heater. For a more detailed description of cantilever design see [13].

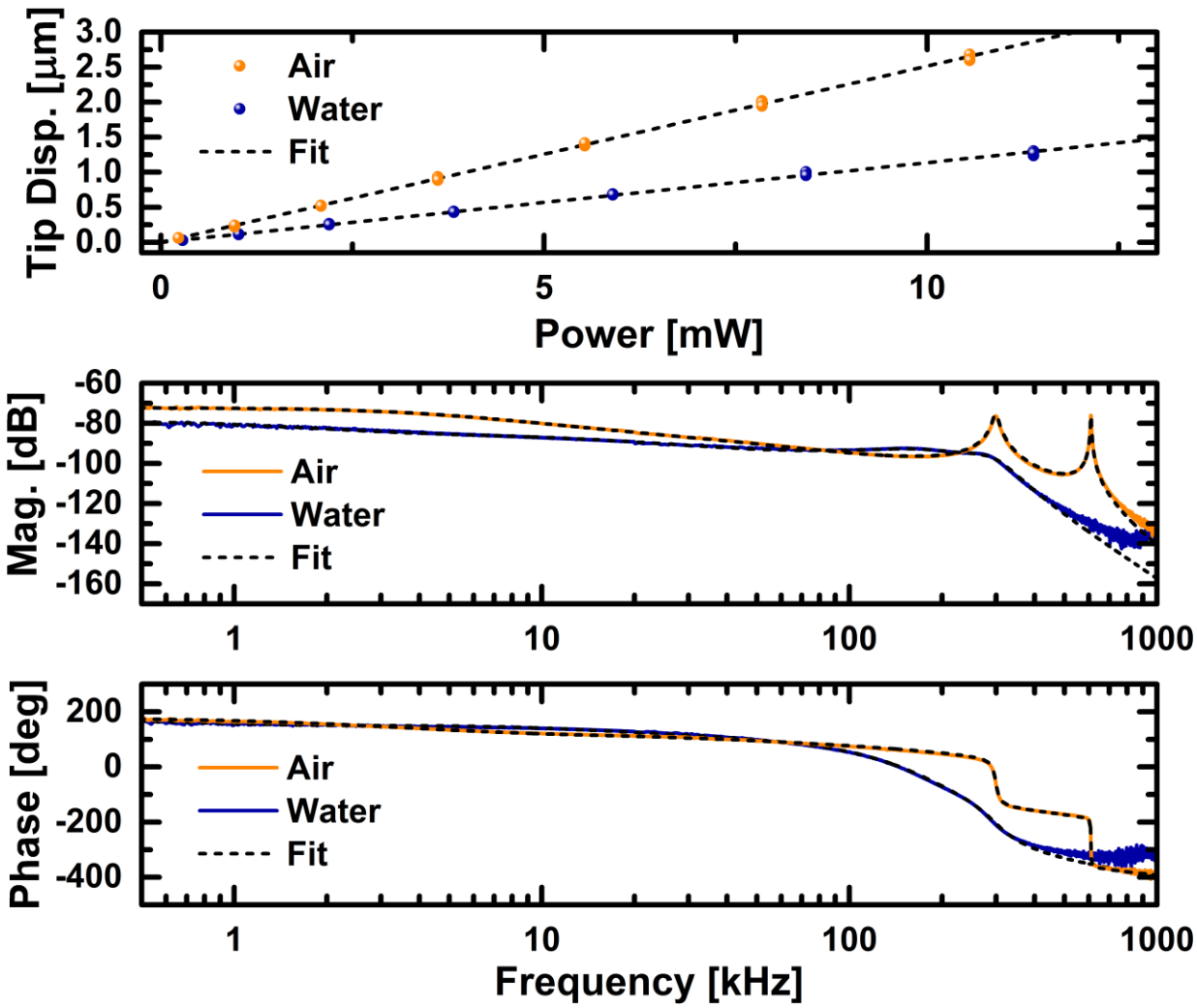

Figure 2: Top: Measured cantilever tip displacement in air and water as a function of dissipated power. For each power level 5 measured tips displacements are plotted on top of each other. Linear fits visualize the linear behavior of the two systems. Bottom: Measured frequency response (magnitude and phase) of cantilevers operated in air and water and the fitted transfer functions. The first two mechanical resonance modes are well defined in air. In water the two peaks are less well defined due to the larger damping by the water.

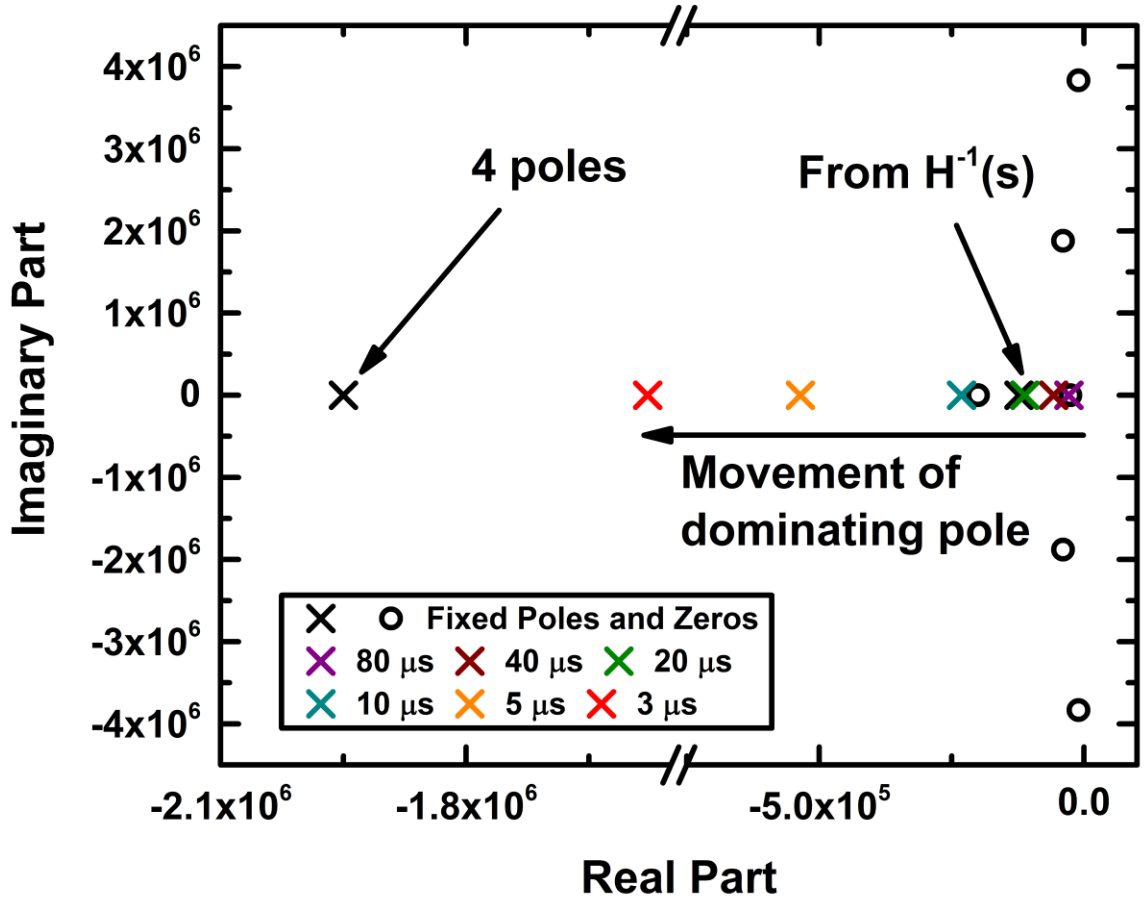

Figure 3: Pole (crosses) and zero (circles) map of the simulated input signals ($X(s) = Y(s)/H(s)$) for operating in air. In the map we find poles and zeros from the inverted transfer function ($H(s)$) and poles from the desired responses ($Y(s)$). The colored crosses represent the position of the dominating pole for 10-90% rise time of 80 µs, 40 µs, 20 µs, 10 µs, 5 µs and 3 µs. 4 identical poles, form the desired response, are places to the left in the plot. The dominating pole of the desired response, is moved from the right to the left in order to reduce the 10-90% rise time. All the poles in the desired responses are place on the real axis to ensure critically damped responses.

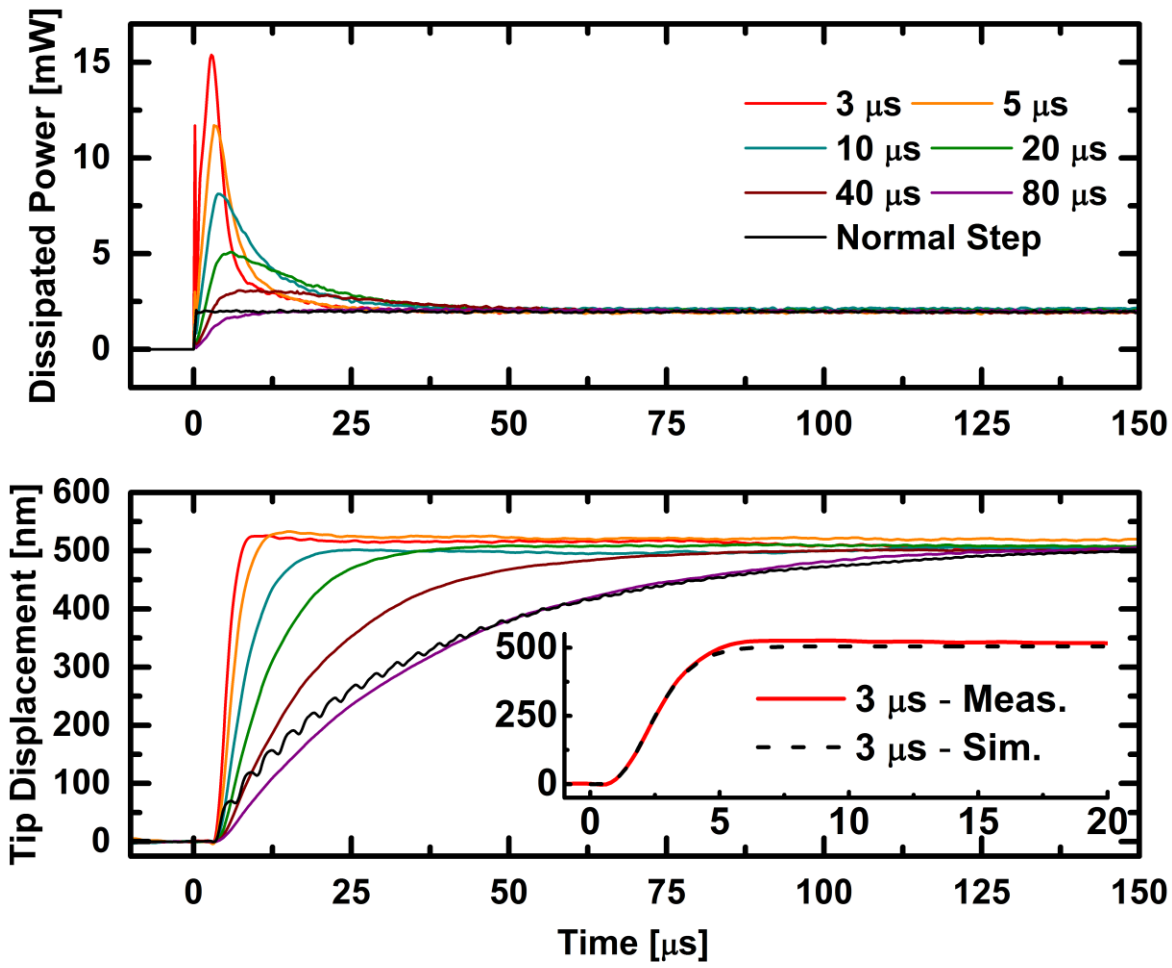

Figure 4: Experimental demonstration of rise time reduction in air. Top: Power dissipated in the actuator as a function of time needed to achieve 10-90% rise times ranging from 3 μs to 80 μs. As the target rise time decreases the overshoot in the dissipated power increases and the shape of it splits into one with two peaks. The peak splitting is need to suppress mechanical ringing. Bottom: Cantilever tip deflection as a function of time while applying input signals (Top) needed to achieve 10-90% rise times of 3 μs to 80 μs. The use of a pre-shaped input signal allows us to reduce the rise time from 85 μs to 3 μs at the cost of an ~3% overshoot. Curve color labeling matches those in the Top plot. Insert: Simulated and measured 3 μs rise time curves shows to be in good agreement.

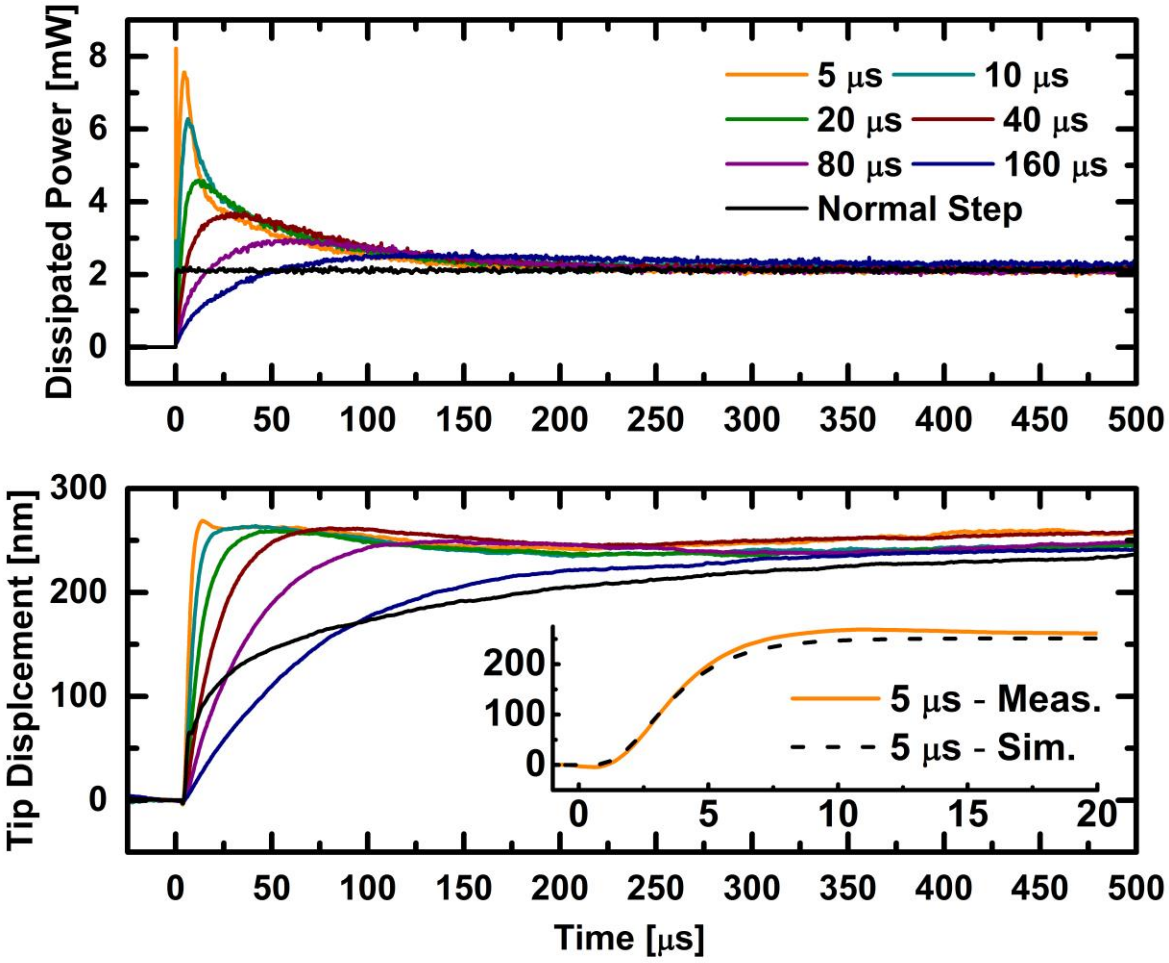

Figure 5: Experimental demonstration of rise time reduction in water. Top: Power dissipated in the actuator as a function of time needed to achieve 10-90% rise times ranging from 5 µs to 160 µs. As the target rise time decreases the overshoot in the dissipated power increases and the shape of it splits into one with two peaks. Bottom: Cantilever tip deflection as a function of time while applying the input signals (Top) needed to achieve 10-90% rise times of 5 µs to 160 µs. The use of pre-shaped drive signal allows us to reduce the 10-90% rise time 234 µs to 5 µs at the cost of a ~5% overshoot. Curve color labeling matches those in the Top plot. Insert: Simulated and measured 5 µs rise time curves are in good agreement.

Table 1: Our description of the frequency response measured in air and water can be divided into 6 components: (i) the gain, (ii) the thermal response, (iii) 1st mechanical response, (iv) 2nd mechanical response, (v) a first order response to improve fitting above 20 kHz and (vi) finally a time delay in the system approximated using a Padé approximation. All the fitting parameters used for each component are listed here.

	Operation in Air	**Operation in Water**
Gain	$243\ \mathrm{nm/mW}$	$114\ \mathrm{nm/mW}$
Thermal Response	$\frac{1}{38 \cdot 10^{-6} \cdot s + 1}$	$\frac{4.63 \cdot 10^{4} \cdot s + 8.01 \cdot 10^{8}}{s^2 + 1.13 \cdot 10^{5} \cdot s + 8.01 \cdot 10^{8}}$
1st Mech. Resonance	$\frac{3.53 \cdot 10^{12}}{s^2 + 7.90 \cdot 10^{4} \cdot s + 3.53 \cdot 10^{12}}$	$\frac{1.21 \cdot 10^{12}}{s^2 + 9.9 \cdot 10^{5} \cdot s + 1.21 \cdot 10^{12}}$
2nd Mech. Resonance	$\frac{1.47 \cdot 10^{13}}{s^2 + 2.11 \cdot 10^{4} s + 1.47 \cdot 10^{13}}$	$\frac{3.46 \cdot 10^{12}}{s^2 + 6.51 \cdot 10^{5} \cdot s + 3.46 \cdot 10^{12}}$
>20 kHz fitting	$\frac{1.63 \cdot s + 25 \cdot 10^{6}}{s + 25 \cdot 10^{6}}$	$\frac{5.75 \cdot s + 2 \cdot 10^{6}}{s + 2 \cdot 10^{6}}$
Padé approx.	$\frac{-s + 2/(6 \cdot 10^{-7})}{s + 2/(6 \cdot 10^{-7})}$	$\frac{-s + 2/(1.25 \cdot 10^{-6})}{s + 2/(1.25 \cdot 10^{-6})}$